Hierarchical Beta Zeolites As Catalysts in α-Pinene Oxide Isomerization

Roman Barakov, Nataliya Shcherban, Päivi Mäki-Arvela, Pavel Yaremov, Igor Bezverkhyy, Johan Wärnå, Dmitry Yu Murzin

ACS Sustainable Chemistry & Engineering

pubs.acs.org/journal/ascecg

Research Article

Hierarchical Beta Zeolites As Catalysts in α-Pinene Oxide Isomerization

Roman Barakov, Nataliya Shcherban, Päivi Mäki-Arvela, Pavel Yaremov, Igor Bezverkhyy, Johan Wärnå, and Dmitry Yu. Murzin*

Cite This: ACS Sustainable Chem. Eng. 2022, 10, 6642−6656

Read Online

ACCESS | Metrics & More | Article Recommendations | Supporting Information

ABSTRACT: Hierarchical beta zeolites obtained in the concentrated reaction mixtures (H_2O/Si = 2.5) and micromesoporous materials synthesized using a dual-template approach from a zeolite beta precursor were rigorously characterized and tested in a sustainable and environmentally friendly process of α-pinene oxide isomerization. The highest yield of *trans*-carveol (42%) with chemopreventive activity of mammary carcinogenesis was achieved over low crystalline micro-mesoporous materials characterized by well-developed mesoporosity, an increased fraction of weak-to-medium Brønsted acid sites and low Brønsted and Lewis acid sites (BAS/LAS) ratio. In turn, highly crystalline hierarchical beta zeolites with a lower mesopore volume and the mesopore surface area, stronger Brønsted acidity, and a higher BAS/LAS ratio favored the formation of campholenic aldehyde (31% yield). The mechanism of the desired product and byproducts formation was discussed and its feasibility was confirmed by kinetic modeling.

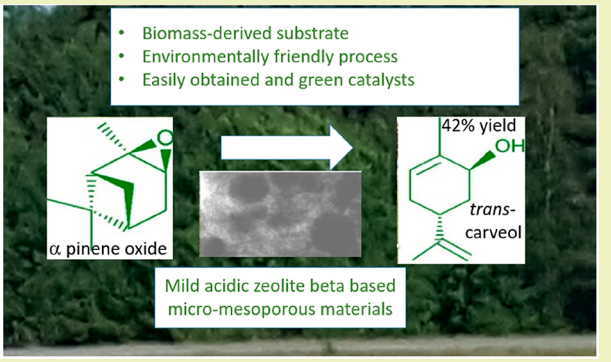

KEYWORDS: *α-Pinene oxide isomerization, Kinetic modeling, trans-Carveol, Campholenic aldehyde, Hierarchical beta zeolites*

INTRODUCTION

Hierarchical zeolites (also called mesoporous zeolites) are considered among the most promising catalytic materials.[1−3] These materials are built from a crystalline network of TO_4 tetrahedra (T = Si, Al) and have uniform micropores inherent to zeolites and secondary porosity, in most cases, associated with mesopores (2−50 nm).[4,5] The presence of mesopores in hierarchical zeolites improves diffusion of the reactants and products and elevates accessibility of catalytically active sites for the bulky molecules.[6] The existence of medium-to-strong and tunable acidity, well-developed mesoporosity in hierarchical zeolites and improved thermal and hydrothermal stability of these materials have led to their successful application as catalysts in a large variety of acid-catalyzed reactions involving bulky organic molecules, such us production of fine chemicals,[7] biomass transformation,[8] catalytic cracking, and petroleum refining.[9]

Beta zeolites find a wide application in industry as a heterogeneous catalyst, mainly in alkylation and acylation,[10] due to good thermal stability and high acidity. For extending the application of beta zeolite to the reactions involving bulky organic molecules, various direct strategies to synthesize hierarchical beta zeolite have been proposed. They can be obtained by utilization of hard templates (e.g., carbon nanoparticles and nanofibers, polystyrene spheres),[11,12] non-ionic (e.g., urea-formaldehyde resin)[13] and cationic polymers (e.g., polydialyldimethylammonium chloride),[14] and silylating agents (phenylaminopropyltrimethoxysilane).[15] Multiquaternary ammonium surfactants[16,17] can be used as mesoporogens to prevent zeolite crystal growth and thereby to stabilize zeolite nanoparticles and nanosheets. Subsequently, after calcination, hierarchical zeolites are formed exhibiting interparticle mesopores. However, synthesis of multiquaternary ammonium surfactants is a costly and labor-consuming process. Hierarchical beta zeolites can also be obtained without additional mesoporogens by a thorough choice of the synthesis conditions (composition and pH of the reaction mixture, temperature, and duration of the hydrothermal treatment).[18] This approach has several drawbacks such as a nonuniform mesopore size distribution, low crystallinity, and a limited concentration of strong Brønsted acid sites in the synthesized materials. One of the perspective pathways to obtain beta nanoparticles with interparticle voids is the hydrothermal treatment of concentrated reaction mixtures (H_2O/Si = 2.5−14) without using of complex poly quaternary ammonium

Received: January 21, 2022
Revised: May 3, 2022
Published: May 12, 2022

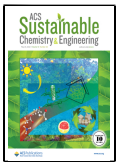

surfactants.[19−22] This synthesis strategy includes abundant zeolite beta nucleation under specific crystallization conditions with further agglomeration and dense packing of the particles limiting their further growth. These materials with well-developed mesoporosity and moderate acidity demonstrated high catalytic activity and selectivity toward the targeted products with pharmacological activities in Prins−Friedel−Crafts reaction of butyraldehyde with 3-buten-1-ol and anisole,[23] Prins cyclization between (−)-isopulegol and acetone,[24] and tetrahydropyranylation of bulky alcohols (1-octadecanol and 1-adamantanemethanol).[22] Another effective route to obtain micromesoporous materials is the assembly of mesostructured materials (SBA-15, KIT-6, MCF) from protozeolitic seeds (the dual-template method) under strongly acidic conditions (pH < 2).[25−27] A highly mesoporous beta/MCF material with mild acidity showed enhanced catalytic activity in verbenol oxide isomerization and allowed to obtain the targeted paramenthanic diol with anti-Parkinson activity in the highest yield (58%) among investigated catalysts.[28,29] The last two approaches can be realized using the same reaction mixture with the pH adjustment and addition of a nonionic surfactant for assembly of protozeolitic seeds providing the additional benefits for practical applications of zeolitic materials.

Terpenes is a sustainable and diverse source for the production of value added chemicals.[30,31] The turpentine oleoresins obtained from coniferous trees and terebinth and the essential oils from citric compounds are the most valuable sources of terpenes. The bicyclic terpenes (α- and β-pinenes) are the main components of wood turpentine.[32] Catalytic epoxidation of α-pinene allows to obtain α-pinene oxide (APO). This oxide isomerizes in the presence of acid catalysts forming various compounds (Scheme 1).[33,34]

The most industrially desired products of APO isomerization are campholenic aldehydes (CA) and *trans*-carveol (TCV). Campholenic aldehyde is regarded as an intermediate for the production of flavor and fragrance chemicals, such as sandalwood-like fragrance, being applied as an odorant in the preparation of perfume and medicines.[35] *trans*-Carveol is a valuable component of the valencia orange essence oil used in the production of flavors and fragrances. This product of APO isomerization also exhibits chemopreventive activity of mammary carcinogenesis.[36] An *α-trans*-dihydroxy derivative of CA possesses potent anti-Parkinson activity in animal models.[37] A large number of publications are devoted to the selective preparation of CA by APO isomerization.[38−43] High selectivity toward CA being 96% at the complete conversion of APO was reached over Lewis acidic Ti-MCM-22 catalyst in nonpolar solvent (toluene) at 70 °C.[44] However, isomerization of APO into TCV has not been adequately investigated. *trans*-Carveol was obtained in the yield up to 45% using molecularly imprinted polymers,[45] H- and Fe-modified zeolite beta catalysts[46] and ZSM-5 based micromesoporous materials[47] in polar basic solvents (e.g., *N*,*N*-dimethylacetamide, *N*,*N*-dimethylformamide). Lower formation of CA in polar basic solvents can be associated with an interaction of the molecules of basic solvent with strong Lewis acid sites of the catalysts.[46,48] Selectivity toward TCV up to 90% at complete conversion was achieved over heteropoly acids,[49,50] silica-supported heteropoly acids,[51] silica-supported cerium and tin catalysts,[52] and Ce-modified MCM-41 and SBA-15[53] in polar basic solvents. High solubility of heteropoly acids in such solvents and leaching problems with cerium and tin catalysts imply that the synthesis of TCV was performed with homogeneous catalysts[49,52] leading to significant issues, such as laborious catalyst separation and regeneration, toxic waste, and corrosion. Recently, it was shown that sulfonic acid functionalized carbon[54] and phosphonate acid-functionalized carbon spheres[55] were efficient catalysts for highly selective isomerization of APO to TCV (selectivity 67−85% at the complete conversion, *N*,*N*-dimethylformamide as a solvent, 140−160 °C). Nevertheless, application of a large amount of concentrated sulfuric acid for functionalization of carbon and labor-consuming two-step process of phosphonate functionalized carbon synthesis and also of serious concern hindering implementation of these approaches. Easily synthesized hierarchical beta zeolites and beta-based micromesoporous materials characterized by well-developed mesoporosity, high accessibility of the active sites, and tunable acidity can be promising catalysts for APO isomerization into TCV. The important challenge is to investigate the influence of the type, concentration, and strength of the zeolitic material acid sites on the yields of TCV and CA in this process.

The aim of this work is to assess the impact of pore texture and acidic properties on the catalytic behavior for hierarchical beta zeolites obtained in concentrated reaction mixtures and for micromesoporous materials synthesized by a dual-template synthesis approach from a zeolite beta precursor. This method implies utilization of tetraethylammonium hydroxide as a structure-directing agent and a nonionic surfactant Pluronic P-123. The catalytic properties of developed micromesoporous materials and conventional (microporous) beta zeolite were also compared. According to our knowledge data concerning the application of hierarchical beta zeolites and beta-based micromesoporous materials as catalysts for APO isomerization are absent in the open literature.

Scheme 1. Isomerization of α-Pinene Oxide (APO) (1)[a]

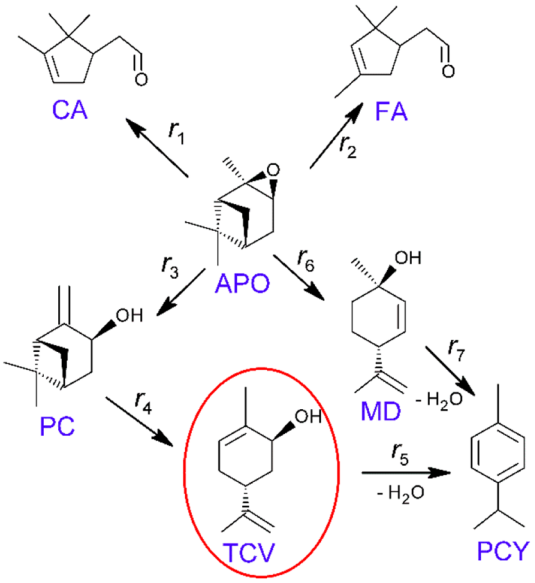

[a]The products are campholenic (CA) (**2**) and fencholenic (FA) (**3**) aldehydes, pinocarveol (PC) (**4**), *trans*-carveol (TCV) (**5**), 2,8-menthadien-1-ol (MD) (**6**), and *p*-cymene (PCY) (**7**).

https://doi.org/10.1021/acssuschemeng.2c00441
ACS Sustainable Chem. Eng. 2022, 10, 6642−6656

EXPERIMENTAL SECTION

Synthesis of the Samples. The samples MZ-1−MZ-3 (MZ, mesoporous zeolite) were obtained in the concentrated beta zeolite reaction mixture (H_2O/Si = 2.5, Si/Al = 25) according to the technique given in refs 22 and 24. Tetraethylammonium hydroxide (TEAOH, 40% aqueous solution, SACHEM, Inc., 5.3 mL) as a template and 0.4 mL of HCl (35 wt %, Sigma-Aldrich) were added to 4.8 mL of H_2O. Then 1.497 g of fumed silica (Aerosil A-175), 0.515 g of as-synthesized aluminum hydroxide gel (9.8 wt % Al_2O_3), and 0.057 g of NaOH (Lach-Ner, 99%) were added to the solution of TEAOH. The obtained reaction mixture was stirred for 1 h. Aluminum hydroxide aqueous suspension was prepared by dissolving $Al(NO_3)_3{\cdot}9H_2O$ (Sigma-Aldrich, 98%) in distilled water followed by adjusting pH to about 7 by adding NaOH solution (20 wt %). $Al(OH)_3$ gel was obtained by washing the suspension with water and subsequent centrifugation. The obtained zeolite reaction mixture ($1SiO_2{:}0.02Al_2O_3{:}0.028Na_2O{:}0.6TEAOH{:}0.2HCl{:}20H_2O$) was concentrated at 75 °C to a H_2O/Si molar ratio in the mixture of 2.5 (Table 1), followed by the hydrothermal treatment (HTT) of the samples in a Teflon-lined autoclave at 140 °C for 2−9 days under static conditions (samples MZ-1−MZ-3, Table 1). The reference sample (CB-1, conventional beta) was obtained under similar conditions (HTT at 140 °C for 7 days, H_2O/Si = 20).

Table 1. Synthesis Conditions, Particle Size, and Relative Crystallinity of the Catalysts in H-Form

sample	H_2O/Si molar ratio	T^a (°C)	τ^b (days)	avg particle size[c] (nm)	relative crystallinity (%)
MZ-1	2.5	140	2	56	55
MZ-2	2.5	140	7	45	75
MZ-3	2.5	140	9	80	85
MZ-4	178	100[d]	1	240	10
MZ-5	178	120[d]	1	330	30
CB-1	20	140	7	450	100

[a] T, temperature of hydrothermal treatment. [b] τ, duration of hydrothermal treatment. [c] From the particle size distribution according to TEM (Figure S3). [d] The beta zeolite reaction mixture was aged at 140 °C for 20 h before hydrothermal treatment in the presence of P-123.

Micromesoporous zeolite-containing materials (MZ-4, MZ-5) were obtained via the dual-template synthesis from zeolite beta precursor in the presence of nonionic surfactant Pluronic P-123 (poly(ethylene glycol)-*block*-poly(propylene glycol)-*block*-poly(ethylene glycol) $HO{-}(CH_2CH_2O)_{20}(CH_2CH(CH_3)O)_{70}(CH_2CH_2O)_{20}H$, Sigma-Aldrich) used for the synthesis of mesoporous cellular foam (MCF). The general procedure for the synthesis of MZ-4 and MZ-5 is given in ref 28. For obtaining the beta zeolite precursor, the reaction mixture for the synthesis of CB-1 was aged at 140 °C for 20 h under static conditions. Then the precursor was added to the solution using for synthesis of MCF and stirred at 40 °C for 24 h. This solution was obtained by adding 3.14 g of P-123 and 8.1 mL of HCl (35 wt %) to 50.8 mL of distilled water at 40 °C, and then adding 3.6 mL of 1,3,5-trimethylbenzene (TMB, Sigma-Aldrich, 98%). Then the obtained gel ($1SiO_2{:}0.02Al_2O_3{:}0.028Na_2O{:}0.6TEAOH{:}0.027P$-123:4.77HCl:1.27TMB:$178H_2O$) with pH < 1 was subjected to HTT in a Teflon-lined stainless steel autoclave at 100 °C (MZ-4, Table 1) or 120 °C (MZ-5) for 24 h under static conditions.

All obtained samples of MZ and sample CB-1 (in Na form) were subjected to a standard procedure (washing with distilled water, drying at 100 °C, calcination at 550 °C for 5 h with the rate 2 °C/min, two times ion-exchange in 1 M NH_4Cl solution at 40 °C for 24 h, and heating to 550 °C for 5 h with the rate 2 °C/min) to obtain the H-form.

Characterization. X-ray diffractometer D8 ADVANCE (Bruker AXS) with Cu K_α radiation was used for analysis of the phase composition of the obtained samples. The relative crystallinity of the calcined samples was evaluated by measuring the ratio of the area under the peak in the 2θ = 20−24° range in the PXRD pattern of the studied samples and CB-1 with the largest area in this range.[56] The crystallinity was considered to be one for CB-1.

Fourier spectrometer Spectrum One (PerkinElmer) was used for measuring FTIR spectra of the obtained samples (pellets with KBr, 1:100).

Energy-dispersive X-ray spectroscopy (the MIRA-3 instrument) was used for determining the content of Si and Al in the obtained samples.

Field emission SEM MIRA-3 (Tescan) with the accelerating voltage of 1−30 kV, and a secondary electron detector was used for obtaining SEM images of the samples. The recording was carried out after loading the samples on the conductive graphitized support. Field emission TEM JEM-2100F (JEOL), with an accelerating voltage of 200 kV, was used for obtaining TEM images. The dispersion of the sample in ethanol was deposited onto a copper grid coated with an amorphous carbon film.

The analyzer of porous materials, Sorptomatic 1990 (Thermo Electron Corp.), was used for measuring nitrogen adsorption by a volumetric method (−196 °C, up to 1 atm). The measurements were carried out after evacuation ($P \leq 0.7$ Pa) of the sample at 350 °C for 5 h. The micropore and mesopore volumes and mesopore surface area (including also the external surface area) were calculated using the comparative *t-plot* method. The micropore size was evaluated by the method of Saito-Foley. The mesopore size was determined from the desorption branch of the isotherm using the method of Barrett−Joyner−Halenda (BJH). For comparison, the mesopore size was also determined from the adsorption branch of the isotherm (BJH). The specific surface area S_{BET} was calculated using the BET equation.

The nature, strength, and total concentration of acid sites were characterized using the pyridine adsorption with FTIR-spectral analysis.[57] The samples (thin plates 8−12 mg/cm^2, without binder) were evacuated (P = 1.4 Pa) at 450 °C for 1 h in a cuvette with NaCl windows. Then pyridine was adsorbed at 150 °C for 15 min and desorbed at 150−450 °C (step 50 °C, holding time 30 min). A Fourier spectrometer Spectrum One (PerkinElmer) was used for recording the spectra of the adsorbed pyridine. The integral molar absorption coefficients (ε(LAS) = 2.22 cm/μmol and ε(BAS) = 1.67 cm/μmol)[58] for the absorption bands at 1454 and 1545 cm^{-1}, respectively, were used for evaluating the concentration of the Lewis (LAS) and Brønsted (BAS) acid sites.

The temperature-programmed desorption of ammonia (NH_3-TPD) was also used to investigate the acidic properties of the samples.[59] The catalysts were treated for 30 min in a helium flow at 550 °C with a heating rate of 15 °C/min, cooled to 100 °C, and saturated with ammonia (20 min). Purging with helium at 100 °C was used to desorb the physically bound NH_3. Then NH_3 was desorbed in the temperature range of 100−700 °C (15 °C/min). A gas chromatograph LHM-80 (thermal conductivity detector) was used for recording the NH_3-TPD curve and determining the positions of the desorption maxima. The total amount of desorbed ammonia was determined by dissolving ammonia in water, followed by titrating the ammonium hydroxide with 1 × 10^{-3} mol/L hydrochloric acid solution using an automatic titrating buret. NH_3-TPD curves were deconvoluted using the Gaussian-type peak shape for determining the peak positions of the thermal desorption of NH_3. The average of the acidity values determined from pyridine adsorption and NH_3-TPD gave an error below 5%.

Catalytic Measurements. A batch-mode-operated glass reactor was used to perform isomerization of APO over beta zeolites in the liquid phase. In a typical catalytic experiment, the initial concentration of APO (Aldrich, 97%) was 0.02 mol/L. The catalyst mass and the stirring speed were 75 mg and 390 rpm, respectively. The reaction temperature was 140 °C. *N*,*N*-Dimethylacetamide (Aldrich, ≥99.5%) was used as a solvent (V = 100 mL). Selection of the reaction temperature and the polar solvent, *N*,*N*-dimethylacetamide, was based on several previous studies,[48,54] where it has been confirmed that a polar solvent with a high boiling point and a relatively high reaction

https://doi.org/10.1021/acssuschemeng.2c00441
ACS Sustainable Chem. Eng. 2022, 10, 6642−6656

temperature are beneficial for the formation of *trans*-carveol from α-pinene oxide. Prior to the reaction, the catalyst was treated in the reactor at 250 °C under an inert argon atmosphere for 30 min to diminish its water content.[60] The samples were taken periodically and analyzed with a gas chromatograph (HP 6890) using a HP-5 column (30 m, 320 μm, 0.50 μm), applying the following temperature program: 60 °C (2 min) − 5 °C/min − 280 °C (15 min) and a split ratio of 20:1. The injector temperature was 280 °C, while the detector temperature was 300 °C. The experiments were performed in the kinetic regime using small catalyst particle sizes (90 μm) and high stirring speed.[60,61] GC/MS (Agilent Technologies 6890 N) was used to confirm the reaction products.

The conversion (X) of APO, selectivity (S_i), and the product yields (Y_i) were calculated based on eqs 1−3. Conversion and selectivity were determined using the appropriate reactant and product response factors in the GC analysis determined from multipoint calibration curves. The turnover frequency ("TOF", the number of converted APO molecules per one acid site per unit time) was evaluated based on the total concentration of the acid sites accessible for pyridine molecules according to eq 4.

$$X(\%) = [(C(\mathrm{APO})_0 - C(\mathrm{APO})_t)/C(\mathrm{APO})_0] \times 100 \quad (1)$$

$$S_i(\%) = \left[C_i(\mathrm{product})_t / \sum C_i(\mathrm{product})_t\right] \times 100 \quad (2)$$

$$Y_i(\%) = [X \times S_i]/100 \quad (3)$$

$$\mathrm{TOF}(\mathrm{min}^{-1}) = [n(\mathrm{APO})_0 - n(\mathrm{APO})_{10\mathrm{min}}]/n_{\text{acid sites in75mg catalyst}}/10\ \mathrm{min} \quad (4)$$

$C(\mathrm{APO})_0$ and $C(\mathrm{APO})_t$ are the concentrations (mol/L) of APO in the reaction mixture initially and after a certain time; $C_i(\mathrm{product})_t$ is the concentration (mol/L) of the specific product i at time t; $n(\mathrm{APO})_0$ and $n(\mathrm{APO})_{10\mathrm{min}}$ are the amounts of APO in the reaction mixture initially and after 10 min; $n_{\text{acid sites in 75 mg catalyst}}$ is the amount of BAS and LAS in 75 mg of the catalyst, as determined by FTIR of adsorbed pyridine. The TOF values were calculated after 10 min. The deviations in the product concentrations in repeated catalytic experiments are below 5%, and the analytical error in GC analysis is below 3%.[60]

RESULTS AND DISCUSSION

Catalyst Characterization. *Structure and Morphology.* PXRD patterns of MZ-1−MZ-3 and CB-1 (Figure 1) exhibit a pure *BEA zeolite phase.[62] The diffraction patterns of MZ-4 and MZ-5 also show broad peaks characteristic of beta zeolite. The presence of a low intensity peak at $2\theta = 0.7°$ in the low-angle PXRD patterns of MZ-4 and MZ-5 (Figure 1a) indicates

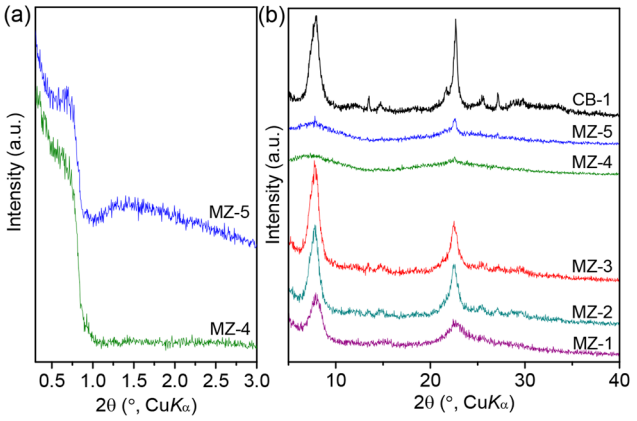

Figure 1. Low-angle (a) and high-angle (b) PXRD patterns of the H-forms of MZ-1−MZ-5 and CB-1 materials.

that these materials have a partially distorted mesoporous structure (mesostructure).

The FTIR spectra of the investigated materials are shown in Figure S1. The absorption bands at 520 and 575 cm^{-1} in the FTIR spectra of MZ-1−MZ-3 and CB-1 is associated with the presence of five- and six-membered rings of $Si(Al)O_{4/2}$ tetrahedra in these samples.[26,63] The presence of these bands also indicates that the MZ samples have a zeolite microstructure. Only one weak band at 570 cm^{-1} is observed in the FTIR spectra of MZ-4 and MZ-5 with a low relative crystallinity (Table 1). The samples MZ-1−MZ-3 contain beta zeolite nanoparticles with a size of 45−80 nm (according to microscopy study, Figures 2, S2, and S3), which are smaller than conventional beta (0.45 μm). A low amount of water in the reaction mixture ($H_2O/Si = 2.5$) facilitates the formation of the zeolite nuclei, which agglomerate, preventing the growth of nanoparticles into large crystals.[20,21,64] The nanoparticle size decreases from 56 to 45 nm with extending the HTT at 140 °C (from 2 to 7 days, samples MZ-1 and MZ-2), which can be associated with the dissolution of the amorphous phase and the formation of particles with a higher crystallinity (75%, Table 1) and a smaller size. Further extending the HTT (MZ-3, 9 days, Table 1) results in an increase in the nanoparticle size up to 80 nm and a relative crystallinity of the material (85%). Changes in the relative crystallinity by PXRD of MZ-1−MZ-3 (Table 1) coincide with the variations in the intensities of the absorption bands at 520 and 575 cm^{-1} in FTIR spectra of these samples (Figure S1).

According to TEM (Figure 2) and SEM (Figure S2) data, the samples MZ-4 and MZ-5 obtained via the dual-template synthesis (TEAOH, P-123) consist of zeolite particles with an average size of 0.24−0.33 μm (Table 1, Figure S3) as well as the amorphous particles with the mesostructure ordering. The increase in the temperature of the HTT (from 100 to 120 °C, samples MZ-4 and MZ-5) results in an increase in the average zeolite particle size and relative crystallinity from 10 to 30% (Table 1) due to a higher crystallization rate at a higher temperature.[28] Thus, the samples MZ-4 and MZ-5 can be referred to as composite materials, featuring both zeolite structure and mesostructure.[65,66]

Textural Properties. Figures 3 and S4 show that N_2 adsorption−desorption isotherms for the obtained samples MZ-1−MZ-5 and MCF are of type IV (according to IUPAC classification).[67] The isotherms of these samples are characterized by a high uptake of N_2 by micropores at a low p/p_0 region (<0.05) and by the presence of a hysteresis loop at p/p_0 0.60−0.97. For MZ-1−MZ-3, the hysteresis loop corresponds to type H_1, which is associated with the nitrogen filing of interparticle pores formed by the agglomeration of zeolite particles. The hysteresis loop of the H_1 type for the samples MZ-4, MZ-5, and MCF is mainly related to the N_2 adsorption in the mesopores of the amorphous aluminosilicate. The isotherm of the conventional beta (CB-1) is of type I, typical for microporous materials with a low external surface area (20 m^2/g). The micropore volume of the obtained samples is dependent on the relative crystallinity and reaches 0.23−0.25 cm^3/g for MZ-1−MZ-3 (Table 2). The micropores of MCF (V_{micro} = 0.04 cm^3/g) are formed by the removal of hydrophilic polyethylene glycol blocks of P-123 that are present in the walls of an as-synthesized sample.[68] Micromesoporous zeolite-containing materials (MZ-4 and MZ-5) with a low-ordered mesostructure are characterized by a larger mesopore volume (1.11−1.33 cm^3/g) and surface area (190−330 m^2/g)

https://doi.org/10.1021/acssuschemeng.2c00441
ACS Sustainable Chem. Eng. 2022, 10, 6642−6656

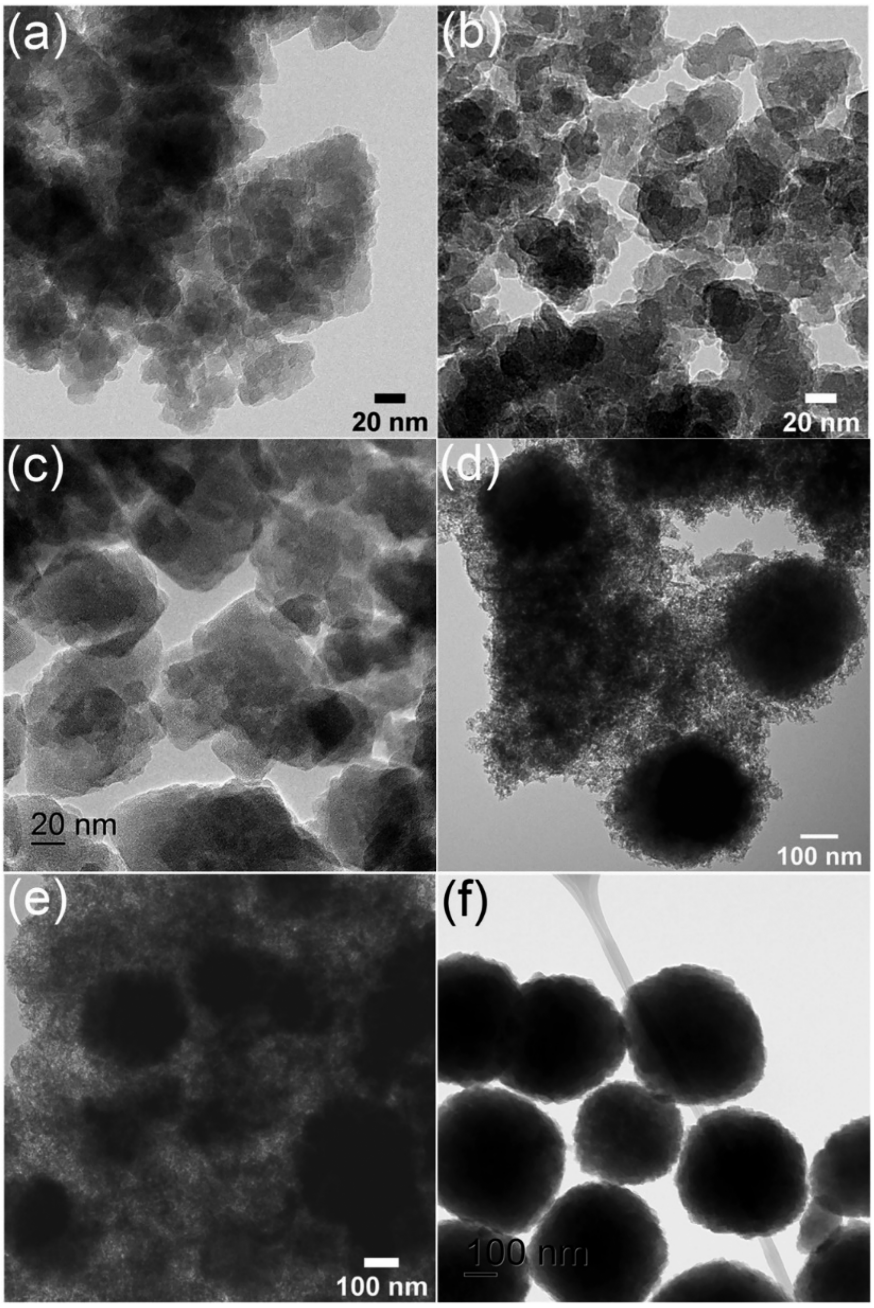

Figure 2. TEM images of the H-forms of MZ-1 (a), MZ-2 (b), MZ-3 (c), MZ-4 (d), MZ-5 (e), and CB-1 (f).

compared to MZ-1−MZ-3 (V_{meso} = 0.43−0.69 cm^3/g, S_{meso} = 85−130 m^2/g, Table 2). The sample MZ-2 with the smallest particle size (45 nm) among hierarchical zeolites MZ-1−MZ-3 (Table 1) possesses an enhanced mesopore volume (V_{meso} = 0.69 cm^3/g, D_{meso} = 36 nm) and surface area (130 m^2/g, Table 2). For comparison, the mesopore size distribution (BJH) curves from the adsorption branch of the isotherms for MB-1−MB-5 samples and MCF are given in Figure S4. The MZ-5 sample obtained at a higher temperature of HTT (120 °C) has a larger mesopore volume (1.33 cm^3/g, D_{meso} = 22 nm) and surface area (330 m^2/g) compared to MZ-4 (HTT at 100 °C). This can be explained by the formation of the mesostructure with a higher degree of condensation of silanol groups during HTT in an acidic media at an elevated temperature.

Chemical Composition and Acidity. Hierarchical zeolites MZ-1−MZ-3, obtained in concentrated reaction mixtures, have a similar chemical composition (Si/Al = 27−31, Table 3) close to the initial reaction mixture (25). For the conventional zeolite beta CB-1, the Si/Al ratio is lower (20) than in hierarchical zeolites. This is associated with the better dissolution of silica species than alumina in the diluted mixture (H_2O/Si = 20) at high pH (ca. 13). On the contrary, a certain part of Al in the beta zeolite precursor is dissolved during the second step of the MZ-4, MZ-5 synthesis in strong acidic media (pH < 1), and the obtained materials have higher Si/Al ratios (48−49) than in the initial reaction mixture (25). In strong acidic media, Al species mainly exist in the form of Al^{3+} rather than the Al oxo form; thereafter, only a few Al species are incorporated in the final materials.[69]

https://doi.org/10.1021/acssuschemeng.2c00441
ACS Sustainable Chem. Eng. 2022, 10, 6642−6656

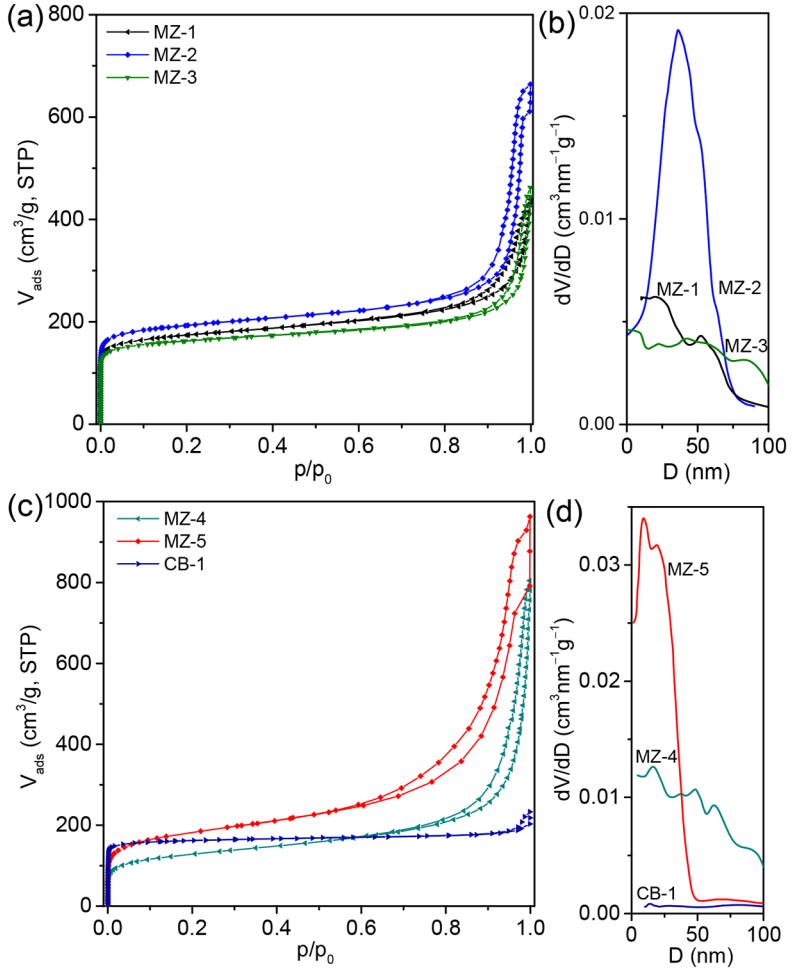

Figure 3. Nitrogen adsorption−desorption isotherms at −196 °C (a, c) and mesopore size distribution (from the desorption branch, BJH method) curves (b, d) for the H-form of MZ-1−MZ-5 and CB-1 materials.

Table 2. Characteristics of the Porous Structure (N_2, −196 °C) of the Materials in the H-Forms

sample	V_{micro} [a] (cm^3/g)	V_{meso} [b] (cm^3/g)	D_{meso} [c] (nm)	S_{meso} [d] (m^2/g)	S_{BET} [e] (m^2/g)
MZ-1	0.24[f]	0.43	50 ± 7	110	670
MZ-2	0.25	0.69	36 ± 15	130	760
MZ-3	0.23	0.46	[g]	85	640
MZ-4	0.13	1.11	[g]	190	490
MZ-5	0.15	1.33	22 ± 14	330	690
CB-1	0.25	0.06	[g]	20[h]	645
MCF	0.04	1.70	9 ± 1	360	470

[a]V_{micro}, micropore volume. [b]V_{meso}, mesopore volume. [c]D_{meso}, mesopore diameter from the desorption branch of the isotherm. Gaussian distribution (standard deviation) is used to estimate the error in the mesopore diameter. [d]S_{meso}, mesopore surface area. [e]S_{BET}, total specific surface area (including also external surface area). [f]Micropore diameter for the samples given in Table 2 is 0.68 nm. [g]Mesopore size distribution without a maximum. [h]The external surface area of beta zeolite.

Table 3. Si/Al Molar Ratio in the Catalysts and Their Acidity by FTIR with Pyridine Adsorption

		BAS concentration (μmol/g)					
sample	Si/Al	weak[a]	medium	strong	total	LAS concn (μmol/g)	total acid sites concn (μmol/g)
MZ-1	27	35	37	35	107	73	180
MZ-2	31	36	40	48	124	62	186
MZ-3	29	28	38	37	103	49	152
MZ-4	48	34	0	0	34	140	174
MZ-5	49	96	48	57	201	132	333
CB-1	20	36	66	156	258	87	345

[a]Weak acid sites: pyridine is desorbed in the range of 150−250 °C; medium acid sites: pyridine is desorbed in the range of 250−350 °C; strong acid sites: pyridine remains after desorption at 350 °C.

FTIR with pyridine adsorption (Table 3, Figure S5) and temperature-programmed desorption of ammonia (NH_3-TPD, Table S1) were used to characterize the acidity of the samples. According to pyridine adsorption, the total acid site concentration in the H-form of the samples MZ-1−MZ-5 is 152−333 μmol/g (Table 3). An increase in the crystallinity of MZ-1−MZ-5 materials is accompanied by a rise in the fraction of medium-to-strong Brønsted acid sites (52% → 73% among total BAS, Table 3) as well as a Brønsted-to-Lewis acid site ratio BAS/LAS (0.2 → 2.1, Table 3). The MZ-4 sample with a low relative crystallinity (10%) possesses only weak Brønsted acid sites (34 μmol/g) in addition to Lewis acid sites (140 μmol/g). The bridging Si−OH−Al groups are referred to as strong Brønsted acid sites, while silanol groups that interacted

https://doi.org/10.1021/acssuschemeng.2c00441
ACS Sustainable Chem. Eng. 2022, 10, 6642−6656

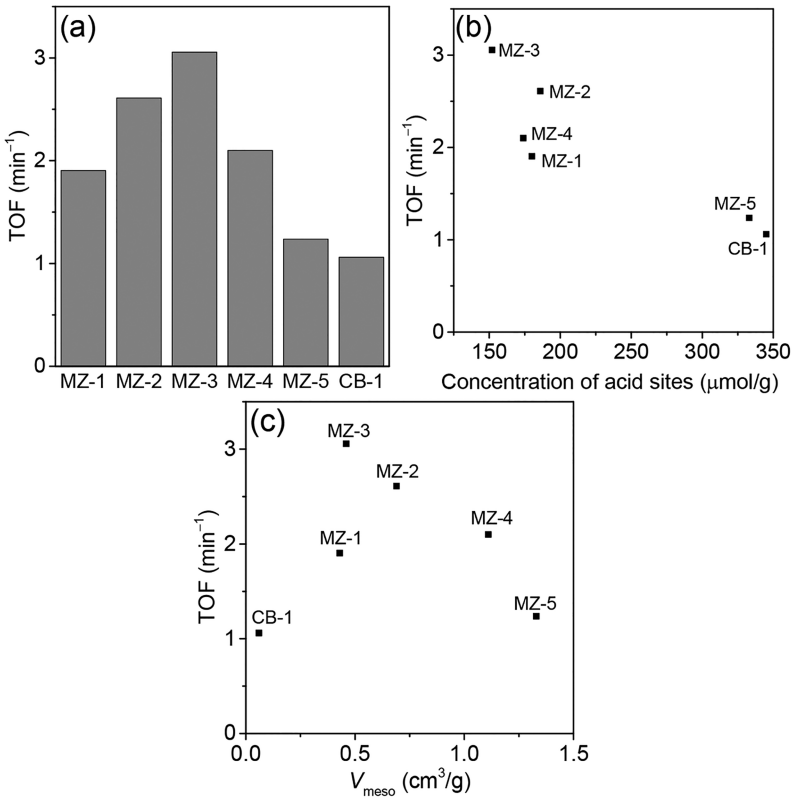

Figure 4. Isomerization of α-pinene oxide: TOF (a) for different catalysts, (b) as a function of total acid site concentration according to pyridine adsorption, and (c) as a function of the catalyst mesopore volume. MZ-1−MZ-5 denote hierarchical beta zeolites and CB-1 conventional beta zeolite. Reaction conditions: 2 mmol of α-pinene oxide, 100 mL of *N*,*N*-dimethylacetamide (solvent), 75 mg of catalyst, 140 °C. TOF was calculated after 10 min of the reaction.

Table 4. Acidity and Catalytic Performance in α-Pinene Oxide Isomerization

		fractions of Brønsted acid sites accessible for pyridine[a] (%)				selectivity at 70% conversion (%)		yield after 3 h (%)		
sample	BAS/LAS	weak[b]	medium	strong	conversion of α-pinene oxide after 3 h (%)	TCV[c]	CA[d]	TCV	CA	C5/C6[e]
MZ-1	1.5	33	34	33	70	37	33	26	23	0.80
MZ-2	2.0	29	32	39	91	35	34	32	30	1.10
MZ-3	2.1	27	37	36	95	35	34	34	31	1.10
MZ-4	0.2	100	0	0	88	44	27	39	24	0.50
MZ-5	1.5	48	24	28	92	45	27	42	25	0.49
CB-1	3.0	14	25	61	89	37	32	34	27	0.87

[a]Fractions were calculated as $[C_B(X)/C_B(\sum)] \times 100\%$, $C_B(X)$ is the concentration of Brønsted weak, medium, or strong acid sites, $C_B(\sum)$ is the total Brønsted acid concentration. [b]Weak acid sites: pyridine is desorbed in the range of 150−250 °C; medium acid sites: pyridine is desorbed in the range of 250−350 °C; strong acid sites: pyridine remains after desorption at 350 °C. [c]*trans*-Carveol. [d]Campholenic aldehyde. [e]C5/C6 is the molar ratio at 70% conversion. C5 products are campholenic and fencholenic aldehydes. C6 products are *trans*-carveol, 2,8-menthadien-1-ol, and *p*-cymene.

with the nearest Al Lewis acid sites are referred to as weak-to-medium Brønsted acid sites.[70]

Microporous beta zeolite (CB-1) features predominantly strong Brønsted acid sites (61% of total BAS) and it is characterized by a high BAS/LAS ratio (3.0). NH_3-TPD data (Table S1 and Figure S6) confirm the results of pyridine adsorption. Samples MZ-2, MZ-3, and CB-1 (with 75−100% relative crystallinity) possess a concentration of medium-to-strong acid sites (240−380 μmol/g, NH_3 desorption maximum > 300 °C) higher than MZ-1, MZ-4, and MZ-5 (84−160 μmol/g), with 10−55% relative crystallinity.

Catalytic Activity of Hierarchical Zeolites in α-Pinene Oxide Isomerization. Hierarchical beta zeolites (MZ-1−MZ-3), micromesoporous aluminosilicates (MZ-4, MZ-5) and conventional beta zeolite (CB-1) were tested in APO isomerization. The highest TOF value was achieved in the presence of the hierarchical zeolite MZ-3 (Figure 4). This is obviously associated with a larger fraction of medium-to-strong Brønsted acid sites in this sample (73% among total BAS, Table 4) compared to other micromesoporous materials (52−71%). Thus, the highest APO conversion is reached over medium-to-strong Brønsted acid sites. Furthermore, the total acid site concentration was the lowest for this catalyst (Figure 4b). The protonation of α-pinene oxide occurs at a lower rate over weak acid sites (Table 4). The lowest TOF value for CB-1 is due to the limited diffusion of α-pinene oxide and reaction

https://doi.org/10.1021/acssuschemeng.2c00441
ACS Sustainable Chem. Eng. 2022, 10, 6642−6656

products in the micropores of the zeolite in the absence of mesopores in its structure (Figure 4a,c). This is also in line with the calculations of the dimensions of *trans*-carveol, which has a minimum value 0.53 × 0.85 nm increasing to 0.77 × 1.09 nm when taking into account van der Waals radius.[40] These values imply diffusional limitations considering that the pore size of beta zeolite is 0.68 nm.[40] The achieved TOF values over investigated catalysts (1.1−3.1 min^{-1}) exceed the corresponding value for a natural zeolite (heulandite, chabazite, and clinoptilolite as main crystallographic phases; TOF = 0.12 min^{-1})[71] due to a higher accessibly of the active sites of beta-based catalysts for α-pinene oxide.

Over 90% conversion of α-pinene was obtained with the catalysts exhibiting both Brønsted and Lewis acid sites and for the most active catalyst the BAS/LAS ratio varied in the range of 1.5−2.1, except MZ-1, which exhibited a slightly lower mesopore volume and less strong Brønsted acid sites than MZ-2, MZ-3, and MZ-5 (Table 4). The highest conversion of APO in the time interval of 1−180 min was achieved when using hierarchical zeolite MZ-3 (Figure 5, 95% conversion after 3 h),

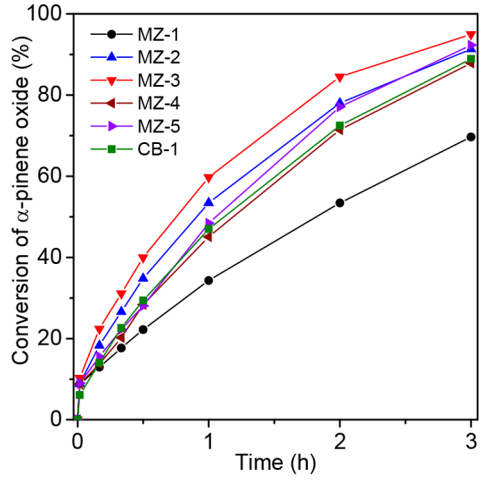

Figure 5. Conversion of α-pinene oxide as a function of reaction time over hierarchical beta zeolites (MZ-1−MZ-5) and conventional beta (CB-1). Reaction conditions: 2 mmol of α-pinene oxide, 100 mL of *N*,*N*-dimethylacetamide (solvent), and 75 mg of catalyst, 140 °C.

which was the most crystalline material (85% relative crystallinity, Table 1) among investigated mesoporous zeolites. The highest activity of MZ-3 material can be explained by the increased concentration of medium and strong acid sites (240 μmol/g, NH_3 desorption maximum at 340 °C) and the presence of interparticle voids (V_{meso} = 0.46 cm^3/g), which contributed to better diffusion of molecules to and from these acid sites, respectively. The second highest conversion, observed for MZ-5 is due to its high mesoporous volume (Table 2). A lower conversion (70−91% after 3 h) was obtained in the presence of a highly crystalline MZ-2, microporous CB-1 catalyst with the increased concentration of the acid sites (251−380 μmol/g, Table S1) and a low crystalline MZ-4 which also exhibited a lower total specific surface area in comparison to MZ-1−MZ-3 and MZ-5. In the presence of MZ-1, conversion of APO reached only 70% after 3 h of the reaction (Table 4) due to a low acid sites concentration (133 μmol/g, according to NH_3-TPD method) and lower mesoporosity (V_{meso} = 0.43 cm^3/g, S_{meso} = 110 m^2/g).

The main targeted products of APO isomerization are *trans*-carveol (TCV) and campholenic aldehyde (CA, Table 4). *trans*-Carveol and other products of APO isomerization (2,8-menthadien-1-ol and *p*-cymene) are referred to C6 products. C5 products are campholenic and fencholenic aldehydes. Low crystalline micromesoporous materials MZ-4 and MZ-5 exhibited the highest selectivity toward TCV (44−45% at 70% conversion of APO) and other product with *para*-menthene structure (2,8-menthadien-1-ol, 18−19% selectivity at 70% conversion) compared to MZ-1−MZ-3 and CB-1 (35−37% selectivity to TCV and 9−13% to MD at 70% conversion). The C5/C6 ratio (0.49−0.50, Table 4) over MZ-4 and MZ-5 was lower than in the presence of MZ-1−MZ-3 and CB-1 (C5/C6 ratio is 0.80−1.10). A high selectivity toward products with the *para*-menthene structure is associated with the increased fraction of weak-to-medium Brønsted acid sites in MZ-4 and MZ-5 (72−100% of total BAS concentration, 40−67% for other samples, Table 4), as well as a low BAS/LAS ratio for these materials (0.2−1.5). Hierarchical zeolites MZ-1−MZ-3 and conventional beta (CB-1) display higher selectivity toward CA (32−34% at 70% conversion of APO) and other C5 product (fencholenic aldehyde, 11−16% at 70% conversion) than MZ-4 and MZ-5 (27% and 5% selectivity for both to CA and FA, respectively, at 70% conversion). MZ-1−MZ-3 samples and CB-1 feature stronger Brønsted acid sites (33−61% of strong acid sites among total BAS concentration, Table 4) as well as a higher BAS/LAS ratio (1.5−3.0) compared to MZ-4−MZ-5 (fraction of strong BAS acid sites up to 28% and BAS/LAS ratio up to 1.5). Thus, the C5/C6 molar ratio decreases with increasing the fraction of weak-to-medium BAS in the obtained mesoporous zeolite (Figure 6) and increases with an increasing

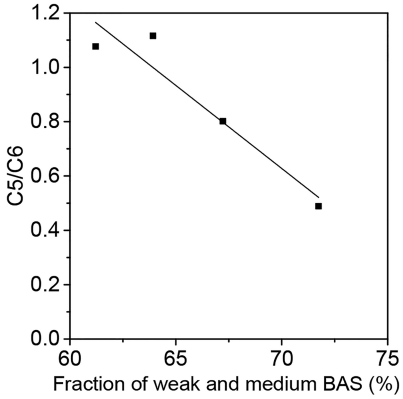

Figure 6. Variation of C5/C6 molar ratio at 70% conversion of α-pinene oxide as a function of the fraction of weak-to-medium BAS in MZ1−MZ-3 and MZ-5 samples. The data for MZ-4 are omitted due to the absence of medium and strong BAS in this sample. The line denotes a trend.

fraction of strong BAS (not depicted here). Moreover, the C5/C6 ratio increases from 0.49 to 1.10 at 70% conversion of APO with an increase of the BAS/LAS ratio from 0.2 to 2.1 for MZ-1−MZ-5 (Table 4). These findings are in a good agreement with the earlier obtained results,[46] reporting the C5/C6 ratio of about 1.7−1.8 at 70% conversion of APO in *N*,*N*-dimethylacetamide as a solvent at 140 °C over commercial H-beta catalysts (Si/Al = 25 and 150) exhibiting the strongest BAS. The lowest C5/C6 ratio (1.20) was obtained over commercial and Fe-modified beta zeolites (Si/Al = 300) with

https://doi.org/10.1021/acssuschemeng.2c00441
ACS Sustainable Chem. Eng. 2022, 10, 6642−6656

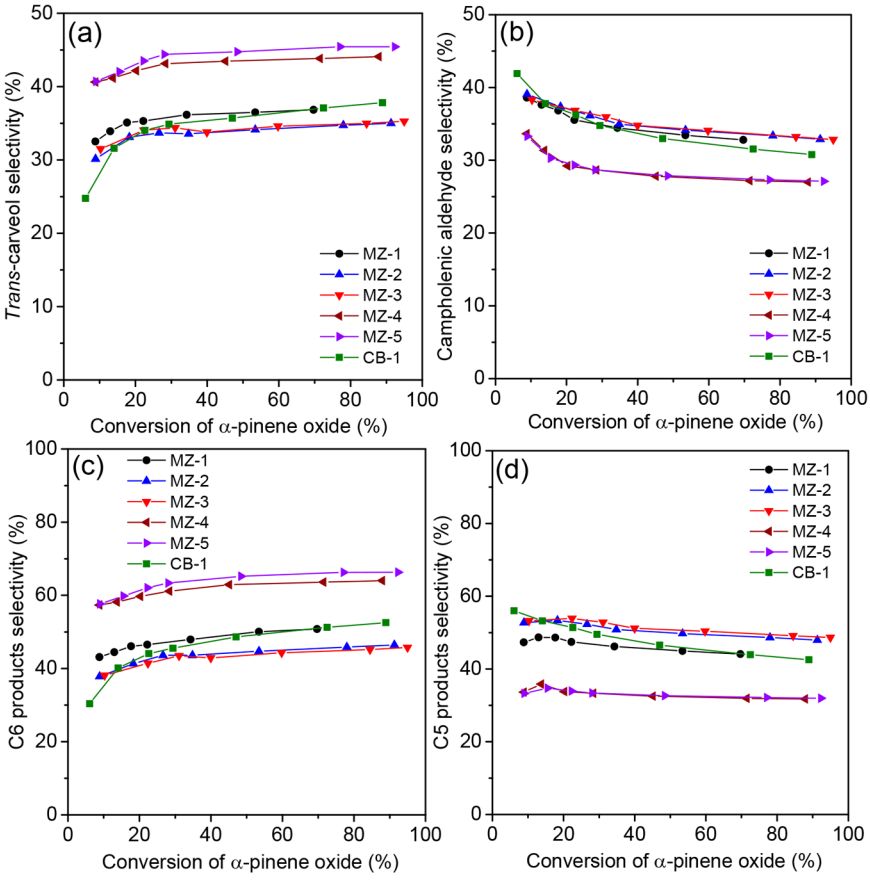

Figure 7. Selectivity to *trans*-carveol (a), campholenic aldehyde (b), C6 (c), and C5 (d) products vs conversion of α-pinene oxide (a) over hierarchical beta zeolites (MZ-1−MZ-5) and conventional beta (CB-1).

weak Brønsted acidity.[46] The C5/C6 ratio also increases from 1.20 to 1.82 for these beta zeolites with elevation of the BAS/LAS ratio from 1.2 to 4.1. The other products of APO isomerization over investigated samples are pinocarveol (PC, 1−2% selectivity at 70% conversion of APO) and *p*-cymene (ca. 2% selectivity at 70% conversion of APO). *p*-Cymene is a product of dehydration of the compounds with the *para*-menthene structure (TCV and MD).

Selectivity dependence on APO conversion over investigated catalysts is depicted in Figure 7. Selectivity toward TCV increases with an increase of APO conversion (Figure 7a), while the selectivity to other C6 products (MD and *p*-cymene) is almost constant (Figure S7a,d). The total selectivity toward C6 products increases with APO conversion (Figure 7c). In turn, the selectivity toward CA decreases and FA increases with conversion of APO (Figures 7b and S7b). The total selectivity toward these products (C5 products) does not change significantly as the reaction proceeds (Figure 7d). Selectivity to PC over investigated catalysts decreases from 14 to 1% during the APO conversion (Figure S7c). According to these changes in selectivity to the products with APO conversion, it can be assumed that C5 products are formed in parallel fashion with C6 products and pinocarveol (PC), at the same time TCV is generated at least partially through adsorbed PC. Selectivity to *p*-cymene, formed via dehydration of *trans*-carveol, was very minor, below 2% (Figure S7d). The thermodynamic analysis performed previously[48] indicated that the Gibbs free energies for formation of different products apart from *p*-cymene formation were negative not reflecting the product distribution. Subsequently the kinetic control linked to catalyst properties determines selectivity to different products.

When comparing the performance of MZ-5 with the data published in the literature (Table S2), it can be stated that even higher selectivity to TCV was obtained over sulfonated carbon[54] and phosphonate supported on carbon spheres,[55] being 82% and 67% at complete conversion of α-pinene oxide. In a previous study[54] the acidic N−C−SO_3H catalyst afforded high TCV selectivity at high temperature in a polar basic solvent, *N*,*N*-dimethylformamide (pK_a = 0.5). Analogously phosphonate functionalized Brønsted solid acid catalyst supported on carbon spheres[55] was very selective to TCV formation in the same solvent at 140 °C. In the literature[54] the effect of the catalyst mass was also investigated, not resulting in a linear relationship between the catalyst mass and conversion, which somehow questions if these experiments were performed in a kinetic regime. Furthermore, it is difficult to directly compare performance of hydrophobic carbon supported catalysts with hydrophilic zeolites and mesoporous materials. Based on our earlier studies[46,47] using H-Beta-25, 7MMAS, and AlSi-SBA-15 samples as catalysts, it was interesting to explore if there are any correlations between the ratio of Brønsted to Lewis acid sites and selectivity to TCV. The results shown in Figure S8 illustrate that selectivity to TCV was rather unaffected by the BAS/LAS ratio, while as it was illustrated above (Figure 6), especially strong Brønsted acid sites promoted the formation of cyclic C5 components. These results thus clearly deviate from those reported in refs

https://doi.org/10.1021/acssuschemeng.2c00441
ACS Sustainable Chem. Eng. 2022, 10, 6642−6656

Scheme 2. Plausible Mechanism of α-Pinene Oxide Isomerization Catalyzed by Beta Zeolites[a]

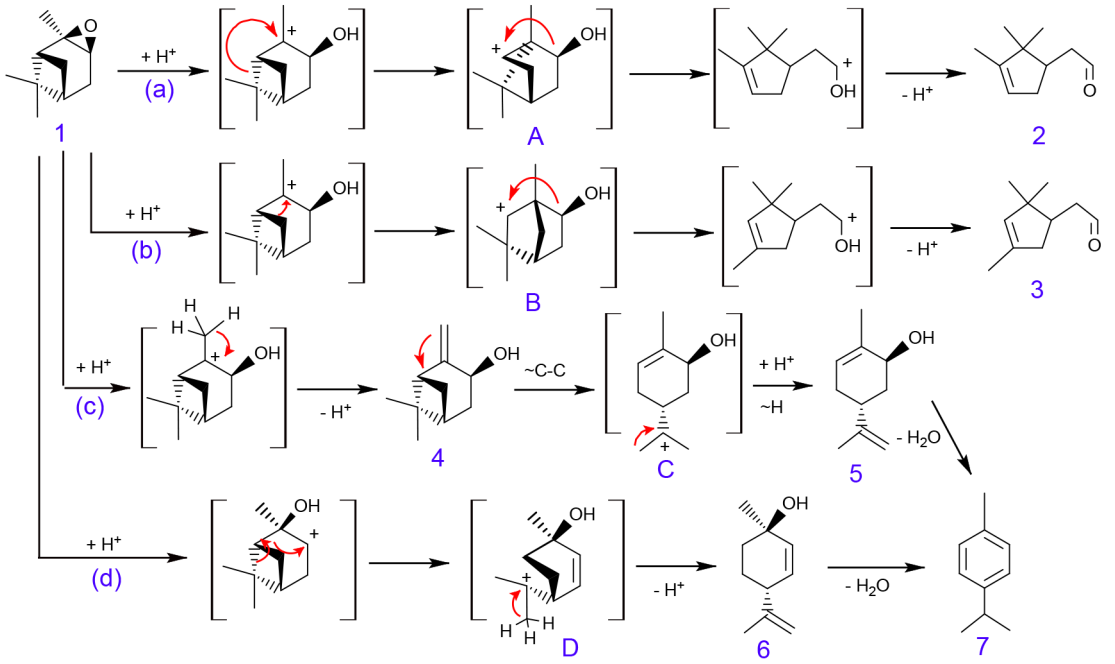

[a]Notation: Routes (a) and (b) require strong Brønsted acid sites, while routes (c) and (d) proceed with weak and medium Brønsted acid sites. Component 1, α-pinene oxide; 2, campholenic aldehyde; 3, fencholenic aldehyde; 4, pinocarveol, 5, *trans*-carveol; 6, 2,8-menthadien-1-ol; 7, *p*-cymene.

54 and 55. MZ-5 catalyst with an increased ratio of weak-to-medium Brønsted acid sites to the total concentration of these sites exhibited a higher selectivity (45%) to TCV at 92% conversion of APO compared to Fe-MCM-41[41] (20% at complete conversion).

Based on selectivity dependence on APO conversion and on the results reported previously on isomerization of APO over H- and Fe-modified beta zeolite,[46] formation of the products can be explained according to the reaction mechanism shown in Schemes 2 and 3. The interaction of a proton (Schemes 2) or a vacant orbital of Lewis acid site (Scheme 3) with the epoxide moiety of APO **1** induces the ring-opening with the formation of a carbenium ion, which can undergo several transformations to form various products. A more detailed mechanism is presented in Scheme 2, while in Scheme 3, for the sake of brevity, just two routes through the same carbocations are presented as in the routes catalyzed by Brønsted sites. Rearrangement of the primary ion can occur via migration of the C^1-C^6 bond to cationic C^2 to form the ion **A** (pathway **a**). Cleavage of the C^2-C^3 bond in this ion and a subsequent loss of a proton leads to the formation of CA **2**. An alternative pathway **b** for conversion of the initially formed carbenium ion is a shift of the C^1-C^7 bond to C^2 and the formation of the ion **B**, which rearranges similar to **A**, giving FA **3**. The generation of PC **4** occurs through a direct hydrogen shift and a proton release (pathway **c**). TCV **5** is formed through adsorbed PC **4**, followed by the formation of a new π bond, the C^1-C^2 hydrogen shift in ion C, and deprotonation. Similar to TCV, MD **6** is generated through protonation of APO **1**, followed by the formation of a new C^1-C^2 π bond, hydrogen shift in ion **D** and a proton release. Both TCV and MD can dehydrate to form *p*-cymene **7**.

Scheme 3. Plausible Mechanism of α-Pinene Oxide Isomerization Catalyzed by Lewis Acid Sites[a]

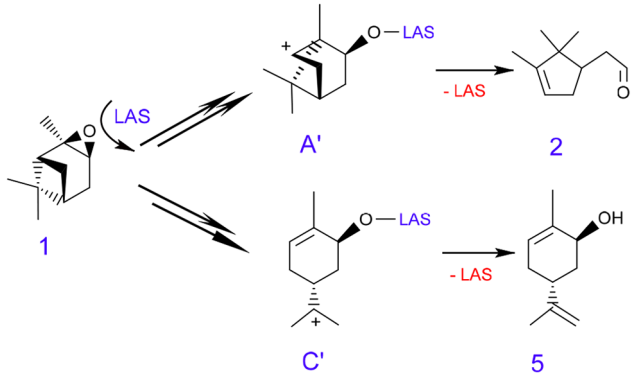

[a]Modified from ref 72. Notation from Scheme 2.

It was suggested[72] that the formation of *trans*-carveol over Lewis acid sites (Scheme 3) occurs through formation of a tertiary cation C′, similar to cation **C** in Scheme 2, which was supposed to be more stable than a secondary cation of type A′. Moreover, high selectivity to TCV can be linked to an easier proton transfer to the tertiary cation in the presence of a basic solvent,[72] such as *N*,*N*-dimethylacetamide applied in the current work. On the contrary, for nonpolar and nonbasic solvents, selectivity to campholenic aldehyde is elevated.[72]

The highest yield of TCV (39−42% after 3 h, Table 4, Figure S9) was achieved over low crystalline micromesoporous materials (MZ-4 and MZ-5). These materials have (1) well-developed mesoporosity and (2) an increased fraction of weak-to-medium Brønsted acid sites among the total concentration of these sites and are characterized by (3) the low BAS/LAS ratio (Table 4). In contrast, highly crystalline hierarchical beta zeolites (MZ-2 and MZ-3) with a lower mesopore volume and

https://doi.org/10.1021/acssuschemeng.2c00441
ACS Sustainable Chem. Eng. 2022, 10, 6642−6656

surface area, stronger Brønsted acidity, and increased BAS/LAS ratio exhibited the highest yield of campholenic aldehyde (31% after 24 h). The increased amount of strong Brønsted acid sites in the catalysts directs the reaction along the routes (a) and (b), on the contrary, the reaction proceeds through the routes (c) and (d) with a lower content of such sites. These findings are consistent with the previously obtained results,[46] reporting that selectivity to TCV and generally to C6 products at complete conversion of APO decreases, and selectivity to CA increases with increasing concentration of the Brønsted acid sites in Fe-modified beta zeolites. The achieved yield of *trans*-carveol (42%) using micromesoporous material MZ-5 is comparable with that obtained previously with other zeolite catalysts, namely, Fe-modified beta zeolite (44%, *N*-methylpyrrolidone as a solvent)[46] and ZSM-5-based micromesoporous material (41%, *N*,*N*-dimethylacetamide as a solvent).[47] Moreover, the yield of *trans*-carveol over MZ-5 outperformed the results obtained with microporous beta (CB-1, 34%) and commercial H-beta (Si/Al = 25, 36%, *N*,*N*-dimethylacetamide as a solvent).[40,46] The yield of *trans*-carveol during the reaction is also higher over MZ-5 compared to CB-1 and commercial H-beta. The improved catalytic performance of the best micromesoporous materials is associated with their enhanced mesopore volume and the mesopore surface area as well as mild acidity. The presence of mesopores in the obtained material improves accessibility of the active sites for the reactants, facilitates diffusion of the reactants and products, and contributes to an increase of the overall reaction rate. The increased fraction of weak-to-medium Brønsted acid sites among total sites in micromesoporous materials promotes formation of the desired product (TCV), while stronger Brønsted acid sites in microporous beta zeolite intensify the formation of C5 products. The latter was related[72] to a more stable tertiary cation leading to *trans*-carveol, while the secondary cyclopentanoic cation is less stable. Subsequently formation of TCV is more thermodynamically controlled, while CA formation is kinetically controlled requiring a more efficient catalysts for its generation with, for example, stronger Brønsted acid sites.[72]

Kinetic Modeling of α-Pinene Oxide Isomerization. The applicability of the proposed mechanism (Scheme 2) of α-pinene oxide isomerization was elucidated by comparison of the estimated parameters in kinetic model for the case of *trans*-carveol formation through pinocarveol (Scheme 1) and parallel routes of *trans*-carveol and pinocarveol formation (Scheme S1). Kinetic modeling for the batch reactor of α-pinene oxide isomerization over MZ-5 catalyst used in this investigation is based on the rate equations developed previously.[48] The assumption of a low coverage of the reactant on the catalyst surface compared to the vacant sites integrated in the equations for Scheme 1 results in first order dependencies of the rates as defined below:

$$r_1 = k_1 \times C_{APO} \quad (5)$$

$$r_2 = k_2 \times C_{APO} \quad (6)$$

$$r_3 = k_3 \times C_{APO} \quad (7)$$

$$r_4 = k_4 \times C_{PC} \quad (8)$$

$$r_5 = k_5 \times C_{TCV} \quad (9)$$

$$r_6 = k_6 \times C_{APO} \quad (10)$$

where k_1−k_6 are the rate constants for the corresponding reactions. To simplify the model and avoid an anticipated correlation between k_5 and k_7, the reaction rate r_7 was neglected.

The mass balances for different compounds (with the notation: APO α-pinene oxide, CA campholenic aldehyde, FA fencholenic aldehyde, PC pinocarveol, TCV *trans*-carveol, MD 2,8-menthadien-1-ol, PCY *p*-cymene) are

$$\frac{dC_{APO}}{dt} = -r_1 - r_2 - r_3 - r_6 \quad (11)$$

$$\frac{dC_{CA}}{dt} = r_1 \quad (12)$$

$$\frac{dC_{FA}}{dt} = r_2 \quad (13)$$

$$\frac{dC_{PC}}{dt} = r_3 - r_4 \quad (14)$$

$$\frac{dC_{TCV}}{dt} = r_4 - r_5 \quad (15)$$

$$\frac{dC_{MD}}{dt} = r_6 \quad (16)$$

$$\frac{dC_{PCY}}{dt} = r_5 \quad (17)$$

The kinetic model of α-pinene oxide isomerization over MZ-5 for Scheme S1, which is slightly different from Scheme 1 in terms of the routes for *trans*-carveol formation, is presented in Supporting Information (eqns S1−S13). The differential equations for both models were solved using the backward difference method. The simplex and Levenberg−Marquardt methods were used for the parameter estimation. Experimentally measured concentrations of APO and the reaction products were compared with the calculations by the numerical data fitting using the optimization and simulation software ModEst.[73] The estimated rate constants and calculated concentrations are shown in Figure 8 and Table 5 for the case when *trans*-carveol is formed from pinacarveol and in Figure S10 and Table S3 for parallel formation of *trans*-carveol and pinocarveol (Scheme S1). In general, a high quality of the model fit (Figures 8 and S10) and the value of the coefficient of determination R^2, defined as the variance of all experimental points from the mean value (ca. 99% for both cases), confirm adequate estimations of experimental results for both models.

A more detailed analysis of the estimated parameters (Tables 5 and S3) illustrates as expected similarity in the rate constants for campholenic and fencholenic aldehydes and 2,8-menthadien-1-ol formation (k_1, k_2, k_6, and k_1', k_2', k_6') for both reaction schemes (Schemes 1 and S1). A low amount of the formed *p*-cymene results in poor identification of the constants k_5 and k_5' and the large standard error, which was also previously observed.[48] However, a large standard error for the rate constant of pinocarveol formation k_3' according to Scheme S1 and a small error for the same rate constant for Scheme 1 (k_3) allows to conclude a higher probability of *trans*-carveol formation through pinocarveol and demonstrate the overall applicability of the proposed mechanism (Scheme 1).

https://doi.org/10.1021/acssuschemeng.2c00441
ACS Sustainable Chem. Eng. 2022, 10, 6642−6656

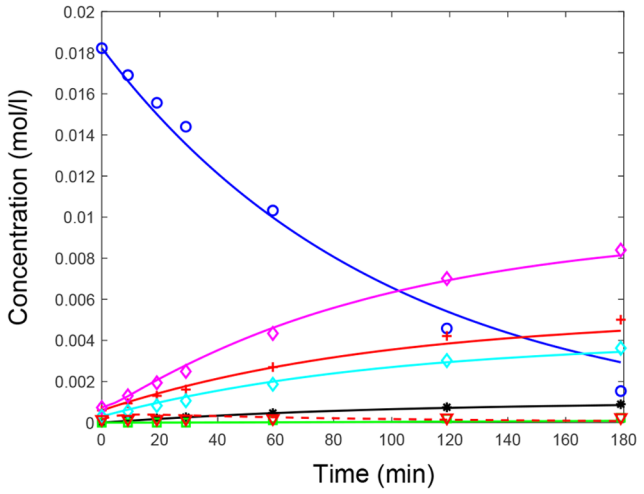

Figure 8. Comparison between experimental (symbols) and calculated (lines) concentrations of reactants and products in α-pinene oxide isomerization over MZ-5 catalyst in the case of *trans*-carveol formation through pinocarveol. Notation: (○, blue) α-pinene oxide, (◊, magenta) *trans*-carveol, (+, red) campholenic aldehyde, (◊, cyan) 2,8-menthadien-1-ol, (*, black) fencholenic aldehyde, (inverted triangle, dashed red) pinocarveol, (□, green) *p*-cymene.

Table 5. Estimated Rate Constants (min^{-1}) for α-Pinene Oxide Isomerization According to Scheme 1 over MZ-5 Catalyst

parameter	estimate	std error	std error (%)
k_1	2.58×10^{-3}	4.42×10^{-4}	17.1
k_2	5.70×10^{-4}	7.39×10^{-5}	13.0
k_3	4.94×10^{-3}	1.98×10^{-4}	4.0
k_4	1.99×10^{-1}	3.57×10^{-2}	17.9
k_5	9.27×10^{-5}	1.33×10^{-4}	>100
k_6	2.10×10^{-3}	1.03×10^{-4}	4.9

CONCLUSIONS

Hierarchical beta zeolites and beta based micromesoporous materials were obtained via hydrothermal treatment of the concentrated reaction mixtures (H_2O/Si = 2.5) and dual-template synthesis from a zeolite beta precursor in the presence of a nonionic surfactant (Pluronic P-123) under strongly acidic conditions, respectively. The mesopore volume and the mesopore surface area decreased while the strength of the acid sites and Brønsted-to-Lewis acid sites ratio BAS/LAS increased with increasing relative crystallinity of the obtained mesoporous zeolites. The obtained materials were tested as sustainable and green catalysts in isomerization of biomass-derived α-pinene oxide at 140 °C in *N*,*N*-dimethylacetamide as a solvent. It was found that the enhanced mesopore volume and the mesopore surface area, an increased fraction of weak-to-medium Brønsted among total acid sites and a low BAS/LAS ratio in beta based micromesoporous materials favored formation of *trans*-carveol (42% yield) with chemopreventive activity of mammary carcinogenesis. A lower mesopore volume and surface area, stronger Brønsted acidity and an increased BAS/LAS ratio in the hierarchical beta zeolites afforded the highest yield of campholenic aldehyde (31% yield). *trans*-Carveol was easily desorbed from weak-to-medium Brønsted acid sites and did not undergo further dehydration to *p*-cymene over stronger sites. Campholenic aldehyde was formed over stronger acid sites and desorbed from these sites without further transformations. A plausible mechanism of α-pinene oxide isomerization catalyzed by beta zeolites was discussed. Kinetic modeling results confirmed that C5 products (campholenic and fencholenic aldehydes) were formed in parallel fashion with C6 products (*trans*-carveol, 2,8-menthadien-1-ol, and *p*-cymene) and the bicyclic compound (pinocarveol), while *trans*-carveol was generated according to kinetic analysis more probably through pinocarveol. The further investigations in the scope of this work will focus on (a) developing new green approaches using biodegradable polymers, amino acids, and so on for synthesis of hierarchically porous zeolites as highly active and selective catalysts of α-pinene oxide isomerization and conversion of other biomass-derived molecules; (b) conducting α-pinene oxide isomerization in the gas phase in a fixed-bed continuous flow reactor combined with *operando* spectroscopy; (c) rational optimization of the reaction conditions of α-pinene oxide isomerization using the full factorial experimental approach.

ASSOCIATED CONTENT

Supporting Information

The Supporting Information is available free of charge at https://pubs.acs.org/doi/10.1021/acssuschemeng.2c00441.

FTIR spectra, SEM images, TEM based particle size distribution of the proton forms, nitrogen adsorption desorption isotherms for MCF, mesopore size distribution, pyridine adsorption FTIR spectra, ammonia TPD profiles and numerical acidity data, selectivity vs conversion data over hierarchical beta zeolites, selectivity to *trans*-carveol as a function of the ratio between Brønsted to Lewis acid concentration, yields of *trans*-carveol and campholenic aldehyde vs time, scheme of α-pinene oxide isomerization with a parallel network, experimental and calculated concentrations of the reactants and products for this scheme, and comparison of the catalytic data in the current work with the literature (PDF)

AUTHOR INFORMATION

Corresponding Author

Dmitry Yu. Murzin − *Johan Gadolin Process Chemistry Centre, Faculty of Science and Engineering, Åbo Akademi University, 20500 Turku, Finland;* orcid.org/0000-0003-0788-2643; Email: dmurzin@abo.fi

Authors

Roman Barakov − *L.V. Pisarzhevsky Institute of Physical Chemistry, National Academy of Sciences of Ukraine, Kyiv 03028, Ukraine*

Nataliya Shcherban − *L.V. Pisarzhevsky Institute of Physical Chemistry, National Academy of Sciences of Ukraine, Kyiv 03028, Ukraine;* orcid.org/0000-0001-8767-702X

Päivi Mäki-Arvela − *Johan Gadolin Process Chemistry Centre, Faculty of Science and Engineering, Åbo Akademi University, 20500 Turku, Finland;* orcid.org/0000-0002-7055-9358

Pavel Yaremov − *L.V. Pisarzhevsky Institute of Physical Chemistry, National Academy of Sciences of Ukraine, Kyiv 03028, Ukraine*

Igor Bezverkhyy − *Laboratoire Interdisciplinaire Carnot de Bourgogne, UMR 6303 CNRS-Université de Bourgogne-Franche Comté, 21078 Dijon, Cedex, France;* orcid.org/0000-0001-8762-6687

https://doi.org/10.1021/acssuschemeng.2c00441
ACS Sustainable Chem. Eng. 2022, 10, 6642−6656

Johan Wärnå − *Johan Gadolin Process Chemistry Centre, Faculty of Science and Engineering, Åbo Akademi University, 20500 Turku, Finland*

Complete contact information is available at: https://pubs.acs.org/10.1021/acssuschemeng.2c00441

Author Contributions

The manuscript was written through contributions of all authors. All authors have given approval to the final version of the manuscript.

Notes

The authors declare no competing financial interest.

■ ACKNOWLEDGMENTS

R.B. and N.S. acknowledge the support of the National Research Foundation of Ukraine to the Project "New effective zeolite catalysts for environmentally friendly processes of the conversion of renewable raw materials into valuable organic compounds" (Project Number 2020.02/0335). N.S. also acknowledges the support of the Verkhovna Rada of Ukraine to a personal scholarship for young scientists - doctors of sciences for 2021. The authors express their gratitude to Valentina Tsyrina (L.V. Pisarzhevsky Institute of Physical Chemistry) for NH_3-TPD.

■ REFERENCES

(1) Kerstens, D.; Smeyers, B.; Van Waeyenberg, J.; Zhang, Q.; Yu, J.; Sels, B. F. State of the Art and Perspectives of Hierarchical Zeolites: Practical Overview of Synthesis Methods and Use in Catalysis. *Adv. Mater.* **2020**, *32*, 2004690.

(2) Chen, L. H.; Sun, M. H.; Wang, Z.; Yang, W.; Xie, W.; Su, B. L. Hierarchically Structured Zeolites: From Design to Application. *Chem. Rev.* **2020**, *120* (20), 11194−11294.

(3) Přech, J.; Pizarro, P.; Serrano, D. P.; Čejka, J. From 3D to 2D Zeolite Catalytic Materials. *Chem. Soc. Rev.* **2018**, *47* (22), 8263−8306.

(4) Čejka, J.; Millini, R.; Opanasenko, M.; Serrano, D. P.; Roth, W. J. Advances and Challenges in Zeolite Synthesis and Catalysis. *Catal. Today* **2020**, *345*, 2−13.

(5) Schwieger, W.; Machoke, A. G.; Weissenberger, T.; Inayat, A.; Selvam, T.; Klumpp, M.; Inayat, A. Hierarchy Concepts: Classification and Preparation Strategies for Zeolite Containing Materials with Hierarchical Porosity. *Chem. Soc. Rev.* **2016**, *45* (12), 3353−3376.

(6) Hartmann, M.; Thommes, M.; Schwieger, W. Hierarchically-Ordered Zeolites: a Critical Assessment. *Adv. Mater. Interfaces* **2021**, *8* (4), 2001841.

(7) Perego, C.; Millini, R. Porous Materials in Catalysis: Challenges for Mesoporous Materials. *Chem. Soc. Rev.* **2013**, *42* (9), 3956−3976.

(8) Mardiana, S.; Azhari, N. J.; Ilmi, T.; Kadja, G. T. M. Hierarchical Zeolite for Biomass Conversion to Biofuel: A Review. *Fuel* **2022**, *309*, 122119.

(9) Sachse, A.; García-Martínez, J. Surfactant-Templating of Zeolites: From Design to Application. *Chem. Mater.* **2017**, *29* (9), 3827−3853.

(10) Tanabe, K.; Hölderich, W. F. Industrial Application of Solid Acid−Base Catalysts. *Appl. Catal. A Gen.* **1999**, *181* (2), 399−434.

(11) Soltanali, S.; Darian, J. T. Synthesis of Mesoporous Beta Catalysts in the Presence of Carbon Nanostructures as Hard Templates in MTO Process. *Microporous Mesoporous Mater.* **2019**, *286*, 169−175.

(12) Sun, M. H.; Chen, L. H.; Yu, S.; Li, Y.; Zhou, X. G.; Hu, Z. Y.; Sun, Y. H.; Xu, Y.; Su, B. L. Micron-Sized Zeolite Beta Single Crystals Featuring Intracrystal Interconnected Ordered Macro-Meso-Micro-porosity Displaying Superior Catalytic Performance. *Angew. Chem., Int. Ed.* **2020**, *59*, 19582−19591.

(13) Li, X.; Shi, Y.; Wang, Z.; Zhang, Y.; Tang, Y. Catalytic Performance of H-β Nanozeolite Microspheres in One-Pot Dynamic Kinetic Resolution of Aromatic Sec-Alcohols. *J. Catal.* **2012**, *288*, 24−32.

(14) Wang, L.; Zhang, Z.; Yin, C.; Shan, Z.; Xiao, F. C. Hierarchical Mesoporous Zeolites with Controllable Mesoporosity Templated from Cationic Polymers. *Microporous Mesoporous Mater.* **2010**, *131* (1−3), 58−67.

(15) Gutiérrez-Rubio, S.; Shamzhy, M.; Čejka, J.; Serrano, D. P.; Moreno, I.; Coronado, J. M. Vapor Phase Acylation of Guaiacol with Acetic Acid over Micro, Nano and Hierarchical MFI and BEA Zeolites. *Appl. Catal. B Environ.* **2021**, *285*, 119826.

(16) Na, K.; Jo, C.; Kim, J.; Cho, K.; Jung, J.; Seo, Y.; Messinger, R. J.; Chmelka, B. F.; Ryoo, R. Directing Zeolite Structures into Hierarchically Nanoporous Architectures. *Science* **2011**, *333* (6040), 328−332.

(17) Liu, B.; Tan, Y.; Ren, Y.; Li, C.; Xi, H.; Qian, Y. Fabrication of a Hierarchically Structured Beta Zeolite by a Dual-Porogenic Surfactant. *J. Mater. Chem.* **2012**, *22* (35), 18631−18638.

(18) Petushkov, A.; Merilis, G.; Larsen, S. C. From Nanoparticles to Hierarchical Structures: Controlling the Morphology of Zeolite Beta. *Microporous Mesoporous Mater.* **2011**, *143* (1), 97−103.

(19) Wang, X.; Li, Y. X.; Luo, C.; Liu, J.; Chen, B. H. Direct Synthesis of Hierarchical Zeolites with Oriented Nanocrystals without Adding Extra Templates. *RSC Adv.* **2013**, *3* (18), 6295−6298.

(20) Möller, K.; Yilmaz, B.; Jacubinas, R. M.; Muller, U.; Bein, T. One-step synthesis of hierarchical zeolite beta via network formation of uniform nanocrystals. *J. Am. Chem. Soc.* **2011**, *133* (14), 5284−5295.

(21) Möller, K.; Yilmaz, B.; Muller, U.; Bein, T. Nanofusion: mesoporous zeolites made easy. *Chem.—Eur. J.* **2012**, *18* (25), 7671−7674.

(22) Barakov, R.; Shcherban, N.; Yaremov, P.; Bezverkhyy, I.; Tsyrina, V.; Opanasenko, M. Hierarchical Beta zeolites obtained in concentrated reaction mixtures as catalysts in tetrahydropyranylation of alcohols. *Appl. Catal. A Gen.* **2020**, *594*, 117380.

(23) Barakov, R.; Shcherban, N.; Yaremov, P.; Bezverkhyy, I.; Čejka, J.; Opanasenko, M. Hierarchical Beta zeolites as catalysts in a one-pot three-component cascade Prins−Friedel−Crafts reaction. *Green Chem.* **2020**, *22* (20), 6992−7002.

(24) Laluc, M.; Barakov, R.; Mäki-Arvela, P.; Shcherban, N.; Murzin, D. Yu. Catalytic activity of hierarchical beta zeolites in the Prins cyclization of (−)-isopulegol with acetone. *Appl. Catal. A Gen.* **2021**, *618*, 118131.

(25) Liu, L.; Pinnavaia, T. J. Assembly of hydrothermally stable aluminosilicate foams and large-pore hexagonal mesostructures from zeolite seeds under strongly acidic conditions. *Chem. Mater.* **2002**, *14* (1), 3−5.

(26) Zhang, D.; Duan, A.; Zhao, Z.; Xu, C. Synthesis, characterization, and catalytic performance of NiMo catalysts supported on hierarchically porous Beta-KIT-6 material in the hydrodesulfurization of dibenzothiophene. *J. Catal.* **2010**, *274* (2), 273−286.

(27) Mei, J.-L.; Shi, Y.; Xiao, C.-K.; Wang, A.-C.; Duan, A.-J.; Wang, X.-L. Hierarchically porous Beta/SBA-16 with different silica-alumina ratios and the hydrodesulfurization performances of DBT and 4,6-DMDBT. *Pet. Sci.* **2022**, *19* (1), 375−386.

(28) Torozova, A.; Maki-Arvela, P.; Shcherban, N. D.; Kumar, N.; Aho, A.; Stekrova, M.; Maduna Valkaj, K.; Sinitsyna, P.; Filonenko, S. M.; Yaremov, P. S.; Ilyin, V. G.; Volcho, K. P.; Salakhutdinov, N. F.; Murzin, D. Y. Effect of acidity and texture of micro-, mesoporous and hybrid micromesoporous materials on the synthesis of paramenthanic diol exhibiting anti-Parkinson activity. *Catal. Struct. React.* **2015**, *1* (3), 146−154.

(29) Shcherban, N. D.; Filonenko, S. M.; Barakov, R. Y.; Sergiienko, S. A.; Yu, K.; Heinmaa, I.; Ivaska, A.; Murzin, D. Y.. New insights in evaluation of acid sites in micro-mesoporous zeolite-like materials using potentiometric titration method. *Appl. Catal. A Gen.* **2017**, *543*, 34−42.

(30) Harman-Ware, A. E. Conversion of Terpenes to Chemicals and Related Products. In *Chemical Catalysts for Biomass Upgrading*; Crocker, M., Santillan-Jimenez, E., Eds.; Wiley-VCH, 2020; pp 529−568, DOI: 10.1002/9783527814794.ch13.
(31) Mewalal, R.; Rai, D. K.; Kainer, D.; Chen, F.; Külheim, C.; Peter, G. F.; Tuskan, G. A. Plant-derived terpenes: a feedstock for specialty biofuels. *Trends Biotechnol.* **2017**, *35* (3), 227−240.
(32) Corma, A.; Iborra, S.; Velty, A. Chemical routes for the transformation of biomass into chemicals. *Chem. Rev.* **2007**, *107* (6), 2411−2502.
(33) Sánchez-Velandia, J. E.; Villa, A. L. Isomerization of α- and β-pinene epoxides over Fe or Cu supported MCM-41 and SBA-15 materials. *Appl.Catal. A Gen.* **2019**, *580*, 17−27.
(34) Sanchez-Velandia, J. E.; Mejia, S. M.; Villa, A. L. Reaction mechanism of the isomerization of monoterpene epoxides with Fe^{3+} as active catalytic specie: A computational approach. *J. Phys. Chem. A* **2020**, *124* (19), 3761−3769.
(35) Brocke, C.; Eh, M.; Finke, A. Recent developments in the chemistry of sandalwood odorants. *Chem. Biodivers* **2008**, *5* (6), 1000−1010.
(36) Crowell, P. L.; Kennan, W. S.; Haag, J. D.; Ahmad, S.; Vedejs, E.; Gould, M. N. Chemoprevention of mammary carcinogenesis by hydroxylated derivatives of d-limonene. *Carcinogenesis* **1992**, *13* (7), 1261−1264.
(37) Ardashov, O. V.; Pavlova, A. V.; Il'ina, I. V.; Morozova, E. A.; Korchagina, D. V.; Karpova, E. V.; Volcho, K. P.; Tolstikova, T. G.; Salakhutdinov, N. F. Highly potent activity of (1R,2R,6S)-3-methyl-6-(prop-1-en-2-yl)cyclohex-3-ene-1,2-diol in animal models of Parkinson's disease. *J. Med. Chem.* **2011**, *54* (11), 3866−3874.
(38) Bruno, S. M.; Valente, A. A.; Pillinger, M.; Amelse, J.; Romao, C. C.; Goncalves, I. S. Gonçalves, Efficient isomerization of α-pinene oxide to campholenic aldehyde promoted by a mixed-ring analogue of molybdenocene. *ACS Sust. Chem. Eng.* **2019**, *7* (16), 13639−13645.
(39) Sánchez-Velandia, J. E.; Villa, A. L. Selective synthesis of high-added value chemicals from α-pinene epoxide and limonene epoxide isomerization over mesostructured catalysts: Effect of the metal loading and solvent. *Catal. Today* **2021**, na DOI: 10.1016/j.cattod.2021.09.011.
(40) Štekrová, M.; Kubů, M.; Shamzhy, M.; Musilová, Z.; Čejka, J. α-Pinene oxide isomerization: role of zeolite structure and acidity in the selective synthesis of campholenic aldehyde. *Catal. Sci. Technol.* **2018**, *8* (9), 2488−2501.
(41) Stekrova, M.; Kumar, N.; Aho, A.; Sinev, I.; Grünert, W.; Dahl, J.; Roine, J.; Arzumanov, S. S.; Mäki-Arvela, P.; Murzin, D. Yu. Isomerization of α-pinene oxide using Fe-supported catalysts: Selective synthesis of campholenic aldehyde. *Appl. Catal. A Gen.* **2014**, *470*, 162−176.
(42) Ravindra, D. B.; Nie, Y. T.; Jaenicke, S.; Chuah, G. K. Isomerisation of α-Pinene Oxide over B_2O_3/SiO_2 and Al-MSU Catalysts. *Catal. Today* **2004**, *96* (3), 147−153.
(43) Liebens, A. T.; Mahaim, C.; Hölderich, W. F.; Blaser, H. U.; Baiker, A.; Prins, R. Selective Isomerization of α-Pinene Oxide with Heterogeneous Catalysts. *Stud. Surf. Sci. Catal.* **1997**, *108*, 587−594.
(44) Pitínová-Štekrová, M.; Eliášová, P.; Weissenberger, T.; Shamzhy, M.; Musilová, Z.; Čejka, J. Highly Selective synthesis of campholenic aldehyde over Ti-MWW catalysts by α-pinene oxide isomerization. *Catal. Sci. Technol.* **2018**, *8* (18), 4690−4701.
(45) Motherwell, W. B.; Bingham, M. J.; Pothier, J.; Six, Y. A study of some molecularly imprinted polymers as protic catalysts for the isomerisation of α-pinene oxide to trans-carveol. *Tetrahedron* **2004**, *60* (14), 3231−3241.
(46) Stekrova, M.; Kumar, N.; Díaz, S. F.; Mäki-Arvela, P.; Murzin, D. Yu. H- and Fe-modified zeolite beta catalysts for preparation of *trans*-carveol from α-pinene oxide. *Catal. Today* **2015**, *241*, 237−245.
(47) Shcherban, N. D.; Barakov, R. Y.; Maki-Arvela, P.; Sergiienko, S. A.; Bezverkhyy, I.; Eranen, K.; Murzin, D. Y. Isomerization of α-pinene oxide over ZSM-5 based micro-mesoporous materials. *Appl. Catal. A Gen.* **2018**, *560*, 236−247.
(48) Mäki-Arvela, P.; Shcherban, N.; Lozachmeur, C.; Russo, V.; Wärnå, J.; Murzin, D. Yu. Isomerization of α-Pinene Oxide: Solvent Effects, Kinetics and Thermodynamics. *Catal. Lett.* **2019**, *149* (1), 203−214.
(49) da Silva Rocha, K. A.; Hoehne, J. L.; Gusevskaya, E. V. Phosphotungstic acid as a versatile catalyst for the synthesis of fragrance compounds by alpha-pinene oxide isomerization: solvent-induced chemoselectivity. *Chem.—Eur. J.* **2008**, *14* (20), 6166−6172.
(50) Ribeiro, C. J. A.; Pereira, M. M.; Kozhevnikova, E. F.; Kozhevnikov, I. V.; Gusevskaya, E. V.; da Silva Rocha, K. A. Heteropoly acid catalysts in upgrading of biorenewables: Synthesis of para-menthenic fragrance compounds from α-pinene oxide. *Catal. Today* **2020**, *344*, 166−170.
(51) da Silva Rocha, K. A.; Kozhevnikov, I. V.; Gusevskaya, E. V. Isomerisation of α-pinene oxide over silica supported heteropoly acid H3PW12O40. *Appl. Catal. A Gen.* **2005**, *294* (1), 106−110.
(52) Costa, V. V.; da Silva Rocha, K. A.; de Sousa, L. F.; Robles-Dutenhefner, P. A.; Gusevskaya, E. V. Isomerization of α-pinene oxide over cerium and tin catalysts: Selective synthesis of *trans*-carveol and *trans*-sobrerol. *J. Mol. Catal. A Chem.* **2011**, *345* (1−2), 69−74.
(53) Stekrova, M.; Kumar, N.; Mäki-Arvela, P.; Ardashov, O. V.; Volcho, K. P.; Salakhutdinov, N. F.; Murzin, D. Yu. Selective Preparation of *T*rans-Carveol over Ceria Supported Mesoporous Materials MCM-41 and SBA-15. *Materials* **2013**, *6* (5), 2103−2118.
(54) Advani, J. H.; Singh, A. S.; Khan, N.-u.H.; Bajaj, H. C.; Biradar, A. V. Black yet green: Sulfonic acid functionalized carbon as an efficent catalyst for highly selective isomerization of α-pinene oxide to *t*rans-carveol. *Appl. Catal. B Environ* **2020**, *268*, 118456.
(55) Singh, A. H.; Advani, J. H.; Biradar, A. V. Phosphonate functionalized carbon spheres as Bronsted acid catalysts for the valorization of bio-renewable α-pinene oxide to *trans*-carveol. *Dalton Trans* **2020**, *49* (21), 7210−7217.
(56) Camblor, M. A.; Corma, A.; Valencia, C. Characterization of nanocrystalline zeolite Beta. *Microporous Mesoporous Mater.* **1998**, *25*, 59−74.
(57) Kim, K.; Ryoo, R.; Jang, H.-D.; Choi, M. Spatial distribution, strength, and dealumination behavior of acid sites in nanocrystalline MFI zeolites and their catalytic consequences. *J. Catal.* **2012**, *288*, 115−123.
(58) Emeis, C. A. Determination of integrated molar extinction coefficients for infrared absorption bands of pyridine adsorbed on solid acid catalysts. *J. Catal.* **1993**, *141* (2), 347−354.
(59) Sandoval-Díaz, L.-E.; González-Amaya, J.-A.; Trujillo, C.-A. General aspects of zeolite acidity characterization. *Microporous Mesoporous Mater.* **2015**, *215*, 229−243.
(60) Faten Díaz, S. Isomerization of pinene epoxides to fine chemicals over metal modified zeolites. *Master Thesis*, Åbo Akademi University, Tuku, Finland, 2011.
(61) Kumar, N.; Mäki-Arvela, P.; Diáz, S. F.; Aho, A.; Demidova, Y.; Linden, J.; Shepidchenko, A.; Tenhu, M.; Salonen, J.; Laukkanen, P.; Lashkul, A.; Dahl, J.; Sinev, I.; Leino, A.-R.; Kordas, K.; Salmi, T.; Murzin, D. Y. Isomerization of α-pinene oxide over iron-modified zeolites. *Topics in Catal.* **2013**, *56* (9), 696−713.
(62) Mintova, S.; Barrier, N. *Verified synthesis of zeolitic materials*; Elsevier, 2016; pp 156−158.
(63) Ali, S. A.; Almulla, F. M.; Jermy, B. R.; Aitani, A. M.; Abudawoud, R. H.; AlAmer, M.; Qureshi, Z. S.; Mohammad, T.; Alasiri, H. S. Hierarchical composite catalysts of MCM-41 on zeolite Beta for conversion of heavy reformate to xylenes. *J. Ind. Eng. Chem.* **2021**, *98*, 189−199.
(64) Zhao, X.; Wang, L.; Guo, P.; Yan, N.; Sun, T.; Lin, S.; Guo, X.; Tian, P.; Liu, Z. Synthesis of high-Si hierarchical beta zeolites without mesoporogen and their catalytic application in the methanol to propene reaction. *Catal. Sci. Technol.* **2018**, *8* (11), 2966−2974.
(65) Vu, X. H.; Bentrup, U.; Hunger, M.; Kraehnert, R.; Armbruster, U.; Martin, A. Direct synthesis of nanosized-ZSM-5/SBA-15 analog composites from preformed ZSM-5 precursors for improved catalytic performance as cracking catalyst. *J. Mater. Sci.* **2014**, *49* (16), 5676−5689.

(66) Dou, B.; Li, J.; Hu, Q.; Ma, C.; He, C.; Li, P.; Hu, Q.; Hao, Z.; Qiao, S. Hydrophobic micro/mesoporous silica spheres assembled from zeolite precursors in acidic media for aromatics adsorption. *Microporous Mesoporous Mater.* **2010**, *133* (1−3), 115−123.
(67) Thommes, M.; Kaneko, M.; Neimark, K.; Olivier, J. P.; Rodriguez-Reinoso, F.; Rouquerol, J.; Sing, K. S. W. Physisorption of gases, with special reference to the evaluation of surface area and pore size distribution (IUPAC Technical Report). *Pure Appl. Chem.* **2015**, *87* (9−10), 1051−1069.
(68) Meynen, V.; Cool, P.; Vansant, E. F. Verified syntheses of mesoporous materials. *Microporous Mesoporous Mater.* **2009**, *125* (3), 170−223.
(69) Liu, H.; Guo, K.; Li, X.; Liu, S.; Gao, X.; Liu, H.; Cao, L.; Chen, Y.; Xu, C. Understanding and direct strategy to synthesize hydrothermally stable micro-mesoporous aluminosilicates with largely enhanced acidity. *Microporous Mesoporous Mater.* **2014**, *188*, 108−117.
(70) Opanasenko, M. V.; Shamzhy, M. V.; Jo, C.; Ryoo, R.; Čejka, J. Annulation of phenols: catalytic behavior of conventional and 2D zeolites. *ChemCatChem.* **2014**, *6* (7), 1919−1927.
(71) Sánchez-Velandia, J. E.; Gelves, J. F.; Márquez, M. A.; Dorkis, L.; Villa, A.-L. Catalytic isomerization of α-pinene epoxide over a natural zeolite. *Catal. Lett.* **2020**, *150* (11), 3132−3148.
(72) Vrbkova, E.; Vyskocilova, E.; Lhotka, M.; Cerveny, L. Solvent influence on selectivity in α-pinene oxide isomerization using MoO_3-modified zeolite BETA. *Catalysts* **2020**, *10* (11), 1244.
(73) Haario, H. *ModEst*, Software for Parameter Estimation, Helsinki, 2001.

https://doi.org/10.1021/acssuschemeng.2c00441
ACS Sustainable Chem. Eng. 2022, 10, 6642−6656